



HAL
open science

Disruption of circumstellar discs by large-scale stellar magnetic fields

Asif Ud-Doula, Stanley Owocki, Nathaniel Dylan Kee

► **To cite this version:**

Asif Ud-Doula, Stanley Owocki, Nathaniel Dylan Kee. Disruption of circumstellar discs by large-scale stellar magnetic fields. *Monthly Notices of the Royal Astronomical Society*, 2018, 478 (3), pp.3049-3055. 10.1093/mnras/sty1228 . hal-02293212

HAL Id: hal-02293212

<https://hal.science/hal-02293212>

Submitted on 24 May 2023

HAL is a multi-disciplinary open access archive for the deposit and dissemination of scientific research documents, whether they are published or not. The documents may come from teaching and research institutions in France or abroad, or from public or private research centers.

L'archive ouverte pluridisciplinaire **HAL**, est destinée au dépôt et à la diffusion de documents scientifiques de niveau recherche, publiés ou non, émanant des établissements d'enseignement et de recherche français ou étrangers, des laboratoires publics ou privés.

Disruption of circumstellar discs by large-scale stellar magnetic fields

Asif ud-Doula,^{1,4★} Stanley P. Owocki² and Nathaniel Dylan Kee³

¹*Penn State Scranton, 120 Ridge View Drive, Dunmore, PA 18512, USA*

²*Bartol Research Institute, Department of Physics and Astronomy, University of Delaware, Newark, DE 19716, USA*

³*Institut für Astronomie und Astrophysik, Eberhard Karls Universität Tübingen, D-72076 Tübingen, Germany*

⁴*LESIA, Observatoire de Paris, 5, place Jules Janssen, F-92195 Meudon, France*

Accepted 2018 May 6. Received 2018 May 2; in original form 2018 March 28

ABSTRACT

Spectropolarimetric surveys reveal that 8–10 per cent of OBA stars harbor large-scale magnetic fields, but thus far no such fields have been detected in any classical Be stars. Motivated by this, we present here magnetohydrodynamical simulations for how a pre-existing Keplerian disc – like that inferred to form from decretion of material from rapidly rotating Be stars – can be disrupted by a rotation-aligned stellar dipole field. For characteristic stellar and disc parameters of a near critically rotating B2e star, we find that a polar surface field strength of just 10 G can significantly disrupt the disc, while a field of 100 G, near the observational upper limit inferred for most Be stars, completely destroys the disc over just a few days. Our parameter study shows that the efficacy of this magnetic disruption of a disc scales with the characteristic plasma beta (defined as the ratio between thermal and magnetic pressure) in the disc, but is surprisingly insensitive to other variations, e.g. in stellar rotation speed, or the mass-loss rate of the star’s radiatively driven wind. The disc disruption seen here for even a modest field strength suggests that the presumed formation of such Be discs by decretion of material from the star would likely be strongly inhibited by such fields; this provides an attractive explanation for why no large-scale fields are detected from such Be stars.

Key words: stars: magnetic field – stars: winds, outflows – MHD – circumstellar matter – stars: early type – stars: emission-line, Be.

1 INTRODUCTION

Modern spectropolarimetric surveys have revealed that 8–10 per cent of massive early-type (OBA) main-sequence stars harbor large-scale (often significantly dipolar) surface fields ranging from about 100 to 10 000 G, with the incidence remarkably constant over a large range of stellar parameters (see e.g. Morel et al. 2015; Wade et al. 2016a). Classical Be stars are a noteworthy exception to this, as no large-scale field has ever been unambiguously detected in this class, despite a sample of roughly 100 closely surveyed stars (Neiner et al. 2012; Wade et al. 2016b). The present paper uses magnetohydrodynamical (MHD) simulations to explore the level of dipole stellar field strength needed to disrupt a Keplerian disc with properties inferred for such Be stars.

A defining characteristic of Be stars is the double-peak emission in Balmer lines arising from a circumstellar decretion disc. This is thought to form from ejection of material (Rivinius, Baade, & Štefl 2003; Kee et al. 2016b) from an underlying star that is rotating at a substantial fraction (generally >70 per cent; Townsend, Owocki, & Howarth 2004) of critical rotation, defined here by the speed

$V_{\text{crit}} = \sqrt{GM/R}$ for material to be in orbit near the equatorial surface radius R . There is substantial observational evidence (e.g. Rivinius, Carciofi, & Martayan 2013, and references therein) to confirm the theoretical expectation that discs around classical Be stars must follow a Keplerian form for orbital speed, $V_{\text{orb}}(r) = V_{\text{crit}}\sqrt{R/r}$. The shear from the associated radially declining orbital frequency $\Omega(r) = V_{\text{orb}}/r = (V_{\text{crit}}/R)(R/r)^{3/2}$ is inherently *incompatible* with the constant, rigid-body form $\Omega_{\text{rot}} = V_{\text{rot}}/R$ that a strong surface magnetic field would impose on ionized plasma near the stellar surface (Townsend & Owocki 2005; ud-Doula, Owocki, & Townsend 2008).

In the case of *accretion* discs (e.g. from protostars, or binary mass exchange), the strong radial decline in field energy, which scales as $B^2 \sim r^{-6}$ for a dipole field (and even more steeply for higher-order fields), means that such *external*¹ magnetic fields can be largely ignored for modelling the inward viscous diffusion from the accretion mass source; thus only in the near-surface regions can the underlying stellar magnetic field substantially influence the

¹Small-scale internal fields generated from the magneto-rotational instability (MRI) likely play a key role in the effective viscous transport of angular momentum that controls accretion.

* E-mail: auu4@psu.edu

Table 1. Stellar and disc parameters for the standard B2e star model.

luminosity	L	5000 L_{\odot}
mass	M	9 M_{\odot}
stellar radius	R	5 R_{\odot}
temperature	T	20,000 K
isothermal sound speed	c_s	16.5 km s ⁻¹
initial peak disc density	ρ_o	10 ^{-11.1} g cm ⁻³
near-star orbital speed	V_{crit}	585 km s ⁻¹
rotation speed at equator	V_{rot}	0.9 V_{crit}
wind mass-loss rate	\dot{M}	1.4 × 10 ⁻¹⁰ M_{\odot} yr ⁻¹

final accretion on to the surface, leading for example to bi-polar jets and/or broader wind outflows (see e.g. Shu et al. 1994; Romanova et al. 2009).

But for Be discs that are thought to arise from the *decretion* of material ejections from the rapidly rotating underlying star, a sufficiently strong field can effectively choke off the formation of any disc before it reaches into a stable Keplerian orbit. This provides a potential rationale for explaining why the large-scale fields inferred for OBA stars are inherently inconsistent with the classical Be phenomenon.

Here we do not attempt to model this complex, generally highly variable decretion process. Instead, the MHD simulations described in Section 2 explore how the introduction of a rotation-aligned dipole field affects a pre-existing Keplerian disc, assuming standard stellar and disc parameters expected for a B2e star (see Section 2.1 and Table 1). A key result (Section 2.2) is that a dipole field with polar strength $B = 100$ G at the stellar surface completely destroys the disc, while a field of $B = 1$ G has little effect. The intermediate, transitional, ‘critical’ case of $B_{\text{crit}} = 10$ G disrupts the *inner* disc, but still leaves some material in Keplerian orbit away from the stellar base. Our parameter studies (Sections 2.3 and 2.4) show surprisingly little effect from varying various parameters, e.g. the equatorial rotation speed V_{rot} (Section 2.4.1) and the mass loss rate \dot{M} from the star’s radiatively driven stellar wind (Section 2.4.2); imposing a split monopole versus dipole field from the stellar surface (Section 2.4.3); and reducing numerical grid resolution in latitude to augment numerical reconnection (Section 2.4.4). But increasing disc *density* or *temperature* requires then a larger field to disrupt the disc, with $B_{\text{crit}}^2 \sim \rho$ or T (Section 2.3). This indicates that the *plasma* β ($\equiv P_{\text{gas}}/P_{\text{mag}} \sim \rho T/B^2$) is a key controlling dimensionless parameter, with the transitional case of $B_{\text{crit}} = 10$ G having $\beta \approx 20$ for disc base gas pressure P_{gas} just above the surface ($r \gtrsim R$) in the equatorial disc mid-plane. We conclude (Section 3) with a brief discussion of the potential implications of our study for magnetic disruption of other kinds of Keplerian discs (e.g. formed from protostellar accretion or binary mass exchange), along with an outlook for future work.

2 MHD SIMULATIONS OF DISC DISRUPTION

2.1 Numerical specifications for a standard B2e model

The MHD simulations here use the same basic code (ZEUS-3D; Stone & Norman 1992) and methods employed in our previous studies of magnetic channelling of radiatively driven stellar winds from OB stars (ud-Doula & Owocki 2002; ud-Doula, Owocki, & Townsend 2008, 2009). Now, however, instead of simply introducing an initial dipole stellar magnetic field to an existing radial wind outflow, we also include a pre-existing Keplerian disc.

This is generated by first defining an analytic disc model with a characteristic peak density ρ_i ($= 2 \times 10^{-11}$ g cm⁻³ in our standard model) in the equatorial mid-plane at the disc base (just above the equatorial stellar surface), with then a power-law radial fall off as $\rho \sim r^{-3.5}$, as expected for a viscous decretion disc (see Kee, Owocki, & Sundqvist 2016a, and references therein). The stratification in height z above a mid-plane radius r is set to a standard Gaussian form $\rho(r, z) = \rho(r, 0) \exp^{-z^2/2H^2}$, where the disc scale height is given by $H = rc_s/V_{\text{orb}}$, with the sound speed $c_s \equiv \sqrt{kT/\mu} \approx 16.5$ km s⁻¹ for our standard isothermal model with fixed temperature $T = 20$ 000 K, and a mean molecular weight μ about 0.6 of a proton mass. Since the near-surface orbital speed $V_{\text{orb}} = V_{\text{crit}} \approx 585$ km s⁻¹ $\gg c_s$, the inner disc is geometrically quite thin, with $H/R \approx 0.028$, and thus an initial full opening angle of just about 3.2 degrees. Because we assume a fixed temperature and sound speed, while the Keplerian orbital speed declines as $V_{\text{orb}}(r) \sim r^{-1/2}$, the outer disc flares up as this opening angle increases with \sqrt{r} .

In our simulations, the surface of the disc also interacts with the radiatively driven stellar wind, leading to a gradual ablation of the disc over time-scales of months or years (Kee et al. 2016a). To minimize here any initial variations from this interaction, we first relax the model with pure hydrodynamical simulations for 1000 ks before introducing any magnetic field, which thus defines the initial time $t = 0$ in our MHD simulations. We additionally use only the radial component of line acceleration, since Kee et al. (2016a) demonstrated that the non-radial components influence the ablation the most. For the standard model, Fig. 1 compares the analytic density distribution for the *disc+wind* with the hydrodynamically relaxed state used as an initial condition for the MHD simulations. This hydrodynamically relaxed disc now has a characteristic peak density $\rho_o = 10^{-11.1}$ g cm⁻³, modestly reduced (by about a factor 0.4) from the value ρ_i for the analytic initial model.

In this standard model, the underlying B2e star is assumed to have a rapid, near-critical rotation $V_{\text{rot}} = 0.9V_{\text{crit}} = 527$ km s⁻¹ (see Table 1), but to avoid ‘staircasing’ effects on wind initiation from an oblate stellar surface (Owocki, Cranmer, & Blondin 1994), we ignore any rotationally induced stellar oblateness, and so simply set all boundary values for field and density at a spherical surface with a fixed stellar radius $R = 5R_{\odot}$. For consistency, we also ignore any gravity darkening in the radiative driving of the stellar wind. As in our previous simulations of wind–field interaction (ud-Doula & Owocki 2002), we use a generalized form of the line-driving formalism of Castor, Abbott, & Klein (1975) (hereafter *CAK*), e.g. to account for integration over the finite stellar cone angle. We choose the line-opacity parameters (k and α in the *CAK* notation, or \bar{Q} and α in the notation developed by Gayley (1995)) so that the stellar luminosity, mass, and radius lead to an overall mass-loss rate $\dot{M} = 1.4 \times 10^{-10} M_{\odot}$ yr⁻¹, thought to be characteristic for our standard B2e star.

As in our previous wind–field simulation models, the lower boundary conditions fix the base density but allow the radial velocity to vary (within an assumption of constant gradient) to adjust to the radiatively driven mass flux. The radial magnetic field is fixed to that of a base dipole, with the latitudinal and azimuthal field allowed to adjust, as needed, to the base wind outflow. The outer boundary conditions simply extrapolate quantities outward, both in the supersonic wind and the stationary disc.

The 2D spherical mesh has 400 radial zones that increase in size by 1 per cent per zone, ranging from the stellar surface radius R to an outer radius of $15R$. The latitudinal grid has 100 zones from pole to pole, with the highest concentration at the equator, set to

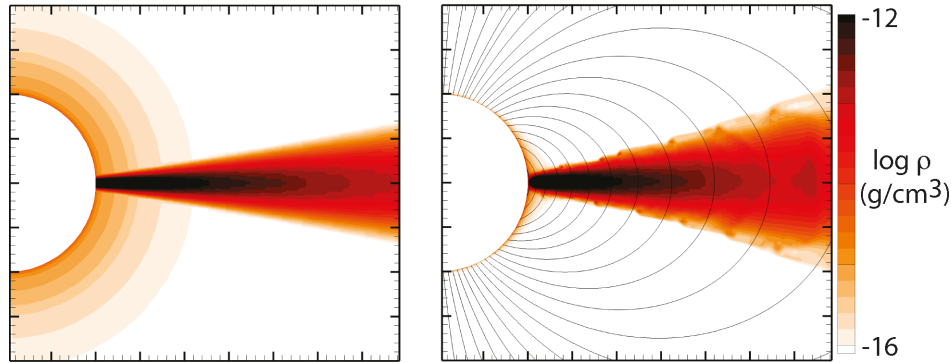


Figure 1. Comparison of the mass density ρ in the analytic model for ***disc+wind (left panel) with the hydrodynamically relaxed state (right panel) that includes the dynamical interaction between the disc and wind. This right panel now also includes the dipole field lines that are applied in the initial condition for the MHD simulations here.

an equatorial step size of 0.01 radian (0.57 degree), which then increases by 4.5 per cent per zone to the poles.

2.2 Results for standard models with $B = 1, 10,$ and 100 G

Within the above specifications for the standard B2e parameters given in Table 1, Fig. 2 shows the spatial variation of density (over 4 dex on a log scale) at time snapshots $t = 500, 1000, 1500,$ and 2000 ks . The upper, middle, and bottom rows compare results for models with polar surface field strengths of $B = 1, 10,$ and 100 G , respectively. Note that the lowest field of just 1 G has only a minor effect on the disc, while the largest field of 100 G completely destroys it; indeed, the remaining equatorial density shown at large times ($t > 1500\text{ ks}$) comes from the magnetically channelled, compressed wind, not from the initial Keplerian disc. For the intermediate, transitional case with a critical field $B_{\text{crit}} = 10\text{ G}$, the inner disc is substantially disrupted, but there remains a significant residual density in the outer disc even at late times.

The disc evolution seen here is the result of a rather complex interaction between the disc and the field, which along the disc surface also includes interaction with the outflowing wind. The entrained field can augment the wind ablation that, even in pure hydrodynamical models, gradually erodes the disc over time-scales of months or years (Kee et al. 2016a). For stronger fields, this erosion become rapid enough to deplete the disc density over dynamical time-scales, leading to feedback that further enhances the disruptive effects of the field, and so results in a complete destruction of the disc for the strong-field case.

The upshot thus seems to be that, for the chosen standard parameters for disc density and temperature, the fields in this range from 1 to 100 G represent a transition from little to full disruption. Let us next examine further how this depends on various assumed parameters for the disc, as well as those associated with the stellar rotation, wind, field configuration, and even numerical grid resolution.

2.3 Parameter study for disc mass evolution

For this broader parameter study, it is helpful to augment the direct plots of the time evolution of density at fixed time snapshots with a rendition of the full time and radius variation of the radial mass distribution $(dm/dr)(r, t)$ of the equatorial disc. As in our previous analysis of magnetic wind channelling from a rotating

star (ud-Doula et al. 2008), we define, for any arbitrary time t , the mass distribution about some latitudinal range (here taken to be $\theta = 90 \pm 10^\circ$) about the equator by

$$\frac{dm}{dr}(r, t) \equiv 2\pi r^2 \int_{80^\circ}^{100^\circ} \rho(r, \theta, t) \sin \theta d\theta. \quad (1)$$

Fig. 3 gives a schematic drawing of this definition.

For the various models of our parameter study, Fig. 4 then shows colourscale renditions of the variation of dm/dr with radius and time over the model simulation range² $r = 1 - 10\text{ R}$ and $t = 0 - 2000\text{ ks}$. The upper row shows again the standard-model cases, now adding intermediate cases with half-dex field increments $B = 10^{1/2}\text{ G}$ and $B = 10^{3/2}\text{ G}$ to the $B = 1, 10,$ and 100 G models discussed above. The colourbar for dm/dr varies logarithmically over 4 decades, with maximum value (red) at $dm/dr = 10^{12}\text{ g cm}^{-1}$ for the standard-model cases, but a factor of 10 higher for models with a 10 times higher base density, as shown in the middle row.

The colourscales for each panel now show quite vividly the contrast and progression between the weak-field limit with little disc disruption ($B = 1\text{ G}$, top left panel) and the strong-field limit with complete disc destruction ($B = 100\text{ G}$, top right panel). The intermediate case with critical field $B_{\text{crit}} = 10\text{ G}$ shows that the near-surface disc is effectively disrupted, but there remains residual material in the outer disc.

As shown in the lower two rows, our study of parameter variations focuses within a half-dex variation about the critical value for partial disc disruption. But now the disc is taken to have either a factor 10 higher base density, $10\rho_0$ (middle row), or an artificially high, factor 10 hotter temperature, $10T = 200\,000\text{ K}$ (lowermost row). Note then that the critical field needed for partial disruption is accordingly now a factor $\sqrt{10}$ higher. Thus models that are a half-dex lower and higher than this critical value now correspond to the weaker versus stronger disc-disruption case of the standard model in the top row.

The very top of each column is labelled with the associated common characteristic value of the plasma beta, defined here as $\beta_0 \equiv (\rho_0 kT/\mu)/(B_{\text{eq}}^2/8\pi)$, where $B_{\text{eq}} = B_{\text{pole}}/2$ is the equatorial value of the magnetic field at the stellar surface. The fact that the overall morphologies within a column are quite similar indicates

²Our simulations generally extend to 15 R , but to avoid occasional backeffects at the outer boundary, we limit analyses to a maximum radius of 10 R , well below any such outer boundary effects.

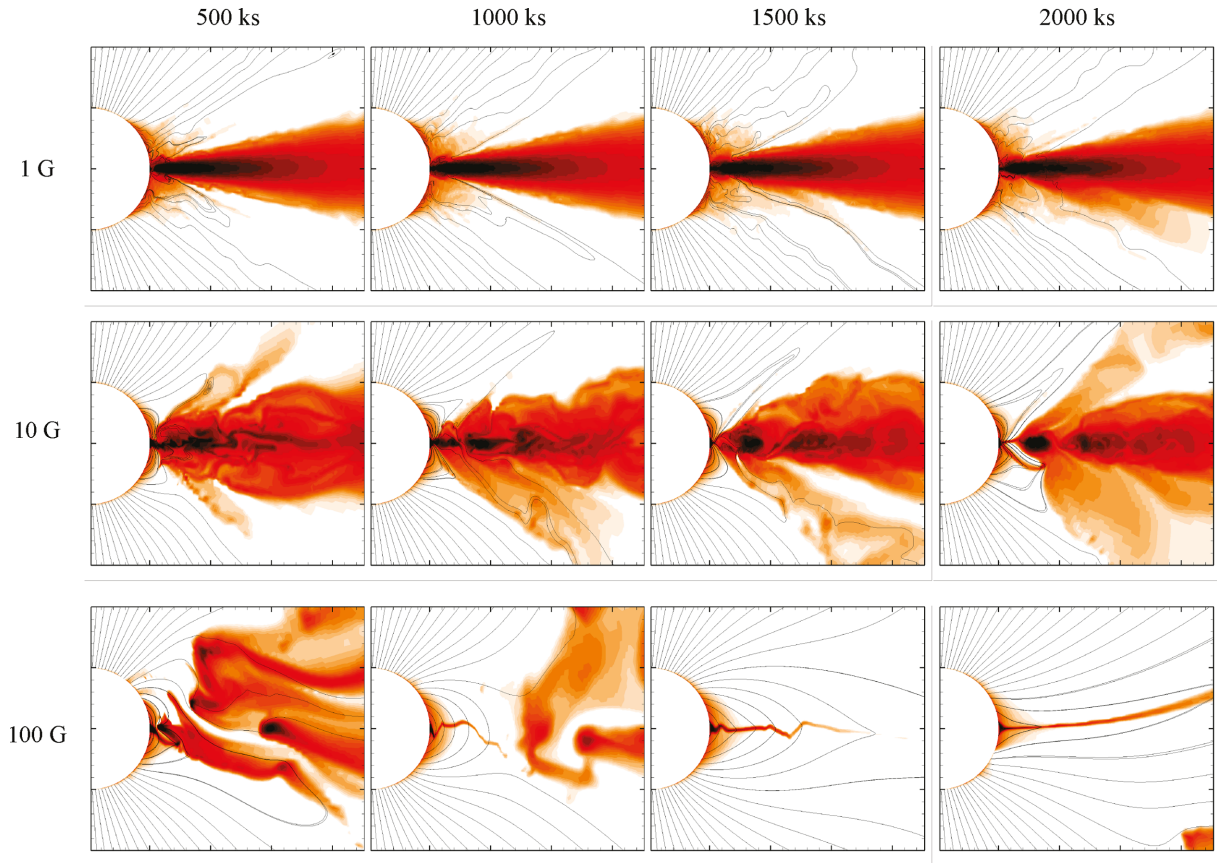


Figure 2. Comparison of disc density for the standard B2e star model with polar field strengths of 1, 10, and 100 G (top, middle, and bottom rows), at time snapshots 500, 1000, 1500, and 2000 ks (left to right columns). The density is rendered on a log scale over the same range as shown by the colourbar in Fig. 1. The lines denote magnetic field from the stellar surface.

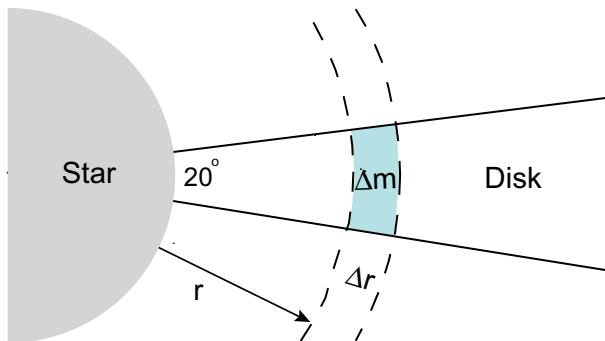


Figure 3. Schematic showing definition of equatorial mass distribution dm/dr as the mass within an angle range of 20° centered on the equatorial disc.

that the plasma beta represents a key controlling parameter for setting the efficacy of magnetic disc disruption.

It may at first seem surprising that the onset, critical case for disruption occurs for a $\beta_o = 20$ that is well above unity, with thus the equatorial magnetic pressure still much smaller than the initial gas pressure at the near-surface disc mid-plane. But of course this initial disc gas pressure is an overall *maximum* value, and so is not really representative of the disc at higher radii, or away from the equator, or indeed at later times after any initial disc erosion. On the other hand, it seems quite appropriate that even for this somewhat

biased definition, a plasma beta of order unity results in the total destruction of the disc, as shown by the uppermost right panel with $\beta_o = 0.2$.

2.4 Relative insensitivity to other parameter variations

We have also explored the effects of varying other parameters that seem plausibly likely to be important for disc disruption, like stellar rotation speed, wind mass-loss rate, field topology, and even numerical grid resolution.

The models shown in Fig. 5 all assume the same critical field value of $B_{\text{crit}} = 10$ G, along with the set of stellar parameters for the standard model with just one specific variation. The leftmost panel reproduces again the dm/dr variation for this critical case of the standard model.

2.4.1 Effect of reduced rotation speed

The next panel to the right shows results for a case with a reduced stellar rotation speed, now set to $V_{\text{rot}} = 0.5V_{\text{crit}}$ (instead of the 90 per cent critical rotation of the standard model). Since the stellar field is rigidly locked to this rotation, this implies a greater relative speed, $\Delta V = \Omega_{\text{rot}}R - V_{\text{crit}}\sqrt{R/r}$, between the rotationally swept stellar field and the orbiting material in the Keplerian disc. For the standard case, this relative speed has a base value $\Delta V = 0.1V_{\text{crit}} = 58.5 \text{ km s}^{-1}$; but in this slower rotation model this

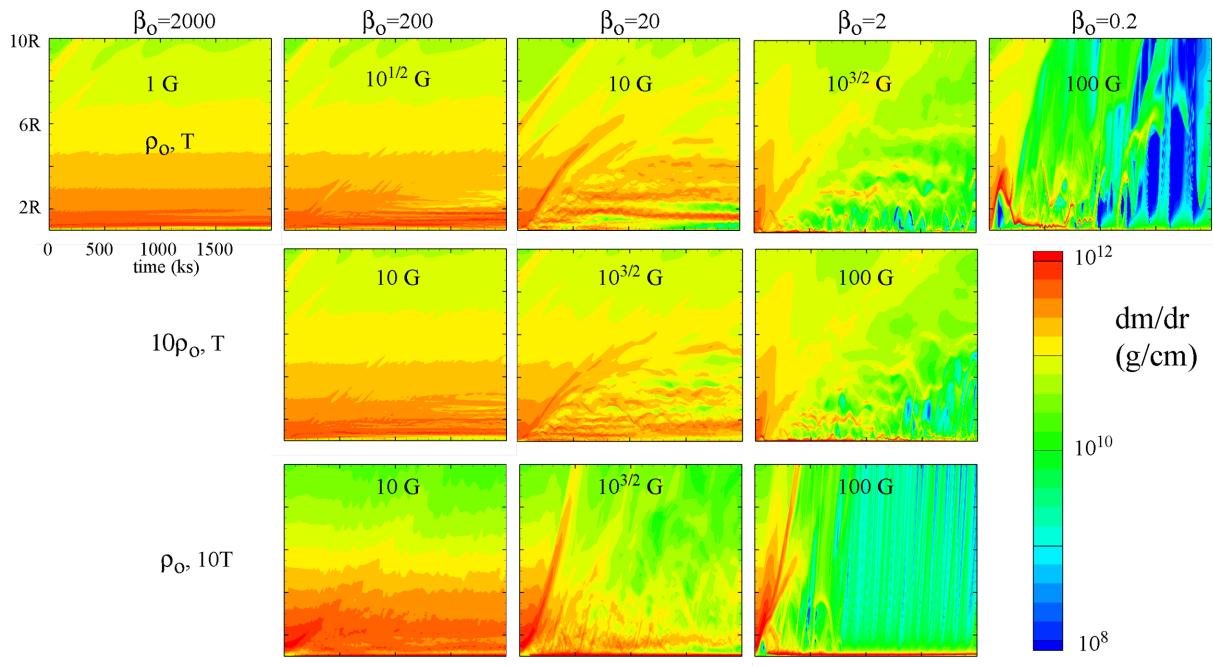


Figure 4. Radius and time evolution of equatorial mass distribution dm/dr , plotted on a log scale with variation of 4 decades from red to blue. The top row shows results for the standard B2e star with a disc base density $\rho_o = 10^{-11.1} \text{ g cm}^{-3}$, labelled by values of the magnetic field at the polar surface. The top left panel shows the disc is largely unaffected by a 1 G field, while the top right panel shows that a 100 G field is sufficient to completely destroy the disc. The middle panel shows the transitional case with a critical field of $B_{\text{crit}} = 10 \text{ G}$ that partially disrupts the disc, effectively removing material from the inner disc, but leaving some of the outer disc still intact. The middle row shows models with 10 times higher base density ρ_o (with colourbar rescaled accordingly), while the bottom row shows models with standard ρ_o but 10 times higher temperature T . Note that both changes require a half-decade increase in field strength to give a similar level of disc disruption as the standard case. This indicates that the plasma beta is a key controlling parameter for such magnetic disruption of the disc. The top label gives the associated numerical values of $\beta_o \equiv (\rho_o k T / \mu) / (B_{\text{eq}}^2 / 8\pi)$, where $B_{\text{eq}} = B/2$ is the equatorial value of the magnetic field at the stellar surface.

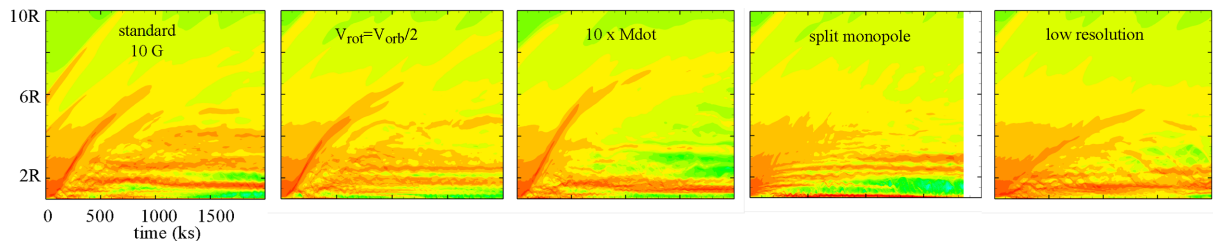


Figure 5. Radius and time evolution of equatorial mass distribution dm/dr for the standard-model case that has the critical field strength $B_{\text{crit}} = 10 \text{ G}$. The leftmost panel for the standard model is compared with various models with just one variation from this standard case. Specifically, the panels progressively to the right show models with lower rotation speed $V_{\text{rot}} = V_{\text{orb}}/2$; 10 times higher wind mass-loss rate; a split monopole (versus dipole) field; and 1/2 the numerical grid resolution in latitude. The similarities in the time and radius evolution of dm/dr among all the panels indicate the magnetic field disruption of the disc is largely insensitive to these parameter variations.

becomes five times higher, $\Delta V = 0.5 V_{\text{crit}} = 292 \text{ km s}^{-1}$, implying a factor 25 increase in the relative kinetic energy. Nonetheless, the dm/dr for this case shown in the second panel from the left appears surprisingly similar, indeed nearly indistinguishable, when compared with the leftmost panel representing the standard case with near-critical rotation.

2.4.2 Effect of increased wind mass loss

The middle panel of Fig. 5 shows a similar insensitivity of magnetic disc disruption to a factor 10 increase in the wind mass-loss rate.

In our previous simulations of the competition between a wind outflow and a stellar dipole field (ud-Doula & Owocki 2002), we identified a dimensionless ‘wind magnetic confinement’ parameter $\eta_* \equiv B_{\text{eq}}^2 R^2 / \dot{M} v_\infty$ (with v_∞ the terminal wind speed in the case of no magnetic field). This sets a characteristic Alfvén radius $R_A \approx \eta_*^{1/4} R$ for maximum closed magnetic loops, with the wind above R_A stretching the dipole field lines open into a radial ‘split monopole’ configuration. Since this reduces the magnetic flux through the equatorial regions of the disc, one might expect that raising or lowering η_* (and thus R_A) would enhance or reduce the magnetic disc disruption. But although the central dm/dr model in Fig. 5

has a factor 10 higher wind mass-loss rate, and thus a factor 10 lower η_* , it nonetheless shows a disc disruption that is still quite similar³ to the standard-model case with a lower \dot{M} . It thus seems, again somewhat surprisingly, that the radiatively driven wind plays at most a relatively minor role in the magnetic disruption of the disc from such a B2e star.

2.4.3 Effect of split monopole field topology

The second panel from the right of Fig. 5 shows a similarly weak effect for a model that actually imposes such a split monopole field topology right from the stellar surface, independent of any effects of the stellar wind. Again, because this effectively eliminates the magnetic flux through the equatorial disc, one would expect this to significantly reduce the magnetic disc disruption. Indeed, the initial evolution for this case does not show the strong initial ejection stream associated with the poloidal field threading the disc; but over the long term, the overall level of disc disruption is similar to what is seen in the standard case with a dipole field. Again, somewhat surprisingly, a monopole versus dipole field topology does not seem to have much effect on the magnetic disruption of the disc.

2.4.4 Effect of reduced grid resolution, and associated enhancement in numerical reconnection

The rightmost panel of Fig. 5 shows a similarly weak effect for a simulation with a factor two reduction in grid resolution (with now only 50 latitudinal zones from pole to pole, but still with a relatively high concentration about the equator). Because this increases the effective scale for numerical reconnection of field lines, and so reduces the effective magnetic Reynolds number, one might expect this would lead to a somewhat weaker coupling between the field and the gas, and so perhaps a reduced level of magnetic disc disruption. But the results for this case in the rightmost panel are again very similar to the leftmost model with standard grid resolution. Within the tested range, the enhanced magnetic dissipation and reconnection in the low-resolution model thus does not seem to have much effect on the disc disruption.

3 DISCUSSION, CONCLUSIONS, AND FUTURE WORK

A key result of the MHD simulations here is that, for typical parameters for a Be star and disc, a modest polar surface field strength of just 10 G is sufficient to substantially disrupt the inner disc, while fields of about 100 G, comparable to upper limits from spectropolarimetric observations, should effectively destroy the disc over about 1000 ks, or a couple dozen near-star orbital periods $P_{\text{orb}} \approx 40 \text{ ks} \approx 0.5 \text{ d}$. Since such fields are thus inherently incompatible with the Keplerian circumstellar discs that give rise to the signature Balmer emission of Be stars, this provides an attractive explanation for why Be stars are essentially never observed to harbor the large-scale fields that are inferred in 8–10 per cent of other, normal OBA stars on the main sequence.

Our parameter study shows, moreover, that the efficacy of magnetic destruction of such Keplerian discs depends mainly on just

³We have also done additional simulations with lower η_* , even below unity, and again find that the wind parameters have little effect on the disc disruption.

the characteristic plasma beta, and is largely insensitive to the variations of other parameters, including stellar rotation speed, wind mass-loss rate, monopole versus dipole field geometry, and reduced grid resolution that augments numerical reconnection. When characterized in terms of the equatorial surface field strength and peak disc density near the stellar surface in the equatorial mid-plane, significant disc disruption can occur for moderately large $\beta_o \approx 20$, with complete destruction for β_o of order unity.

Because Be discs are thought to form from *decretion* of material from the near critically rotating star, any magnetic field that is sufficiently strong to dominate the near-star disc dynamics seems also likely to inhibit the formation of a Keplerian disc by mass ejections and/or eruptions; but further dynamical simulations accounting directly for such mass ejections are needed to confirm this.

The simulations here do not, however, in any way preclude the formation of *accretion* discs around stars with fields that are strong enough to dominate the near-star dynamics; the strong radial decline of field energy ($B^2 \sim r^{-6}$ for a dipole field) means that such external large-scale fields have negligible effect on the outer disc, and thus on the source regions of the accreting disc mass.

But even for such accretion discs, which in principle can have much larger densities, the study here can provide an overall characterization of the field strengths needed to disrupt or erode the inner disc, and thereby perhaps compete with the accretion feeding rate from the outer disc. They thus provide a simple but useful complement to other, more complete simulations of the effect of magnetic fields on the accretion process.

Further work is needed to relax the several simplifying assumptions of the present simulations. Since the disc temperature affects its gas pressure and thus the plasma beta, future simulations should relax the assumption of isothermal plasma to include a realistic energy equation that accounts for the balance between radiative heating from the star and cooling emission from the disc, including a potentially optically thick radiation transport. For the near-critical rotation of Be stars, the assumption of a uniformly bright spherical star should be relaxed to account for the effects of oblateness and gravity darkening. Beyond the present 2D axisymmetric geometry for a rotation-aligned dipole field, future simulations should explore the effect of tilted dipoles, and/or more complex, higher-order multipole fields that are usually more difficult to detect. Each of these generalizations could plausibly alter the nature and efficiency of magnetic disruption of the circumstellar disc, although the relative insensitivity found here for parameter variations beyond the characteristic plasma beta suggests that such generalized models might likewise follow similar overall scaling with field strength through a characteristic disc plasma beta.

Within these caveats, the central conclusion from this study remains that relatively modest large-scale magnetic field strengths near and below the current upper observational limits for Be stars seem likely to disrupt or destroy any circumstellar disc. This thus provides a fundamental rationale for why Be stars remain the only class of early-type stars without any such observationally inferred large-scale organized magnetic fields.

ACKNOWLEDGEMENTS

A.u.D acknowledges support by NASA through Chandra Award numbers GO5-16005X and TM7-18001X issued by the Chandra X-ray Observatory Center which is operated by the Smithsonian Astrophysical Observatory for and on behalf of NASA under contract NAS8-03060.

REFERENCES

- Castor J. I., Abbott D. C., Klein R. I., 1975, *ApJ*, 195, 157
- Gayley K. G., 1995, *ApJ*, 454, 410
- Kee N. D., Owocki S., Sundqvist J. O., 2016a, *MNRAS*, 458, 2323
- Kee N. D., Owocki S., Townsend R., Müller H.-R., 2016b, in Sigut T. A. A., Jones C. E., eds, ASP Conf. Ser. Vol. 506, Bright Emissaries: Be Stars as Messengers of Star-Disk Physics. Astron. Soc. Pac., San Francisco, p. 47
- Morel T., Catsro N., Fossati L., BOB Collaboration, 2015, in Meynet G., Georgy C., Groh J., Stee P., eds, IAU SYMP, Vol 307, New Windows on Massive Stars. Cambridge Univ. Press, Cambridge, p. 342
- Neiner C. et al., 2012, *MNRAS*, 426, 2738
- Owocki S. P., Cranmer S. R., Blondin J. M., 1994, *ApJ*, 424, 887
- Rivinius T., Baade D., Štefl S., 2003, *A&A*, 411, 229
- Rivinius T., Carciofi A. C., Martayan C., 2013, *A&A Rev.*, 21, 69
- Romanova M. M., Ustyugova G. V., Koldoba A. V., Lovelace R. V. E., 2009, *MNRAS*, 399, 1802
- Shu F., Najita J., Ostriker E., Wilkin F., Ruden S., Lizano S., 1994, *ApJ*, 429, 781
- Stone J. M., Norman M. L., 1992, *ApJS*, 80, 791
- Townsend R. H. D., Owocki S. P., 2005, *MNRAS*, 357, 251
- Townsend R. H. D., Owocki S. P., Howarth I. D., 2004, *MNRAS*, 350, 189
- ud-Doula A., Owocki S. P., 2002, *ApJ*, 576, 413
- ud-Doula A., Owocki S. P., Townsend R. H. D., 2008, *MNRAS*, 385, 97
- ud-Doula A., Owocki S. P., Townsend R. H. D., 2009, *MNRAS*, 392, 1022
- Wade G. A., Neiner C., Alecian E., Grunhut J. H., Petit V., MiMeS Collaboration, *MNRAS*, 456, 2
- Wade G. A., Petit V., Grunhut J. H., Neiner C., MiMeS Collaboration, 2016b, in Sigut T. A. A., Jones C. E., eds, ASP Conf. Ser., Vol 506, Bright Emissaries: Be Stars as Messengers of Star-Disk Physics. Astron. Soc. Pac., San Francisco, p. 207

This paper has been typeset from a $\text{\TeX}/\text{\LaTeX}$ file prepared by the author.